Highly Sensitive and Selective Porphyrin-Based Fluorescent Probe for Nanomolar Detection of Cu^{2+} Ions

So-Hyun Shin , Jihyun Kim , Hyungkyu Moon , T. Sheshashena Reddy , Myung-Seok Choi *

Posted Date: 10 April 2026

doi: 10.20944/preprints202604.0723.v1

Keywords: porphyrin sensor; fluorescence; 2,2′-dipicolylamine; metal cation; copper(II) ion

 doi:10.20944/preprints202604.0723.v1

Article

Highly Sensitive and Selective Porphyrin-Based Fluorescent Probe for Nanomolar Detection of Cu^{2+} Ions

So-Hyun Shin [1], Jihyun Kim [1,2], Hyungkyu Moon [1], T. Sheshashena Reddy [1] and Myung-Seok Choi [1,2,*]

[1] Department of Materials Science and Engineering, Konkuk University, 120 Neungdong–ro, Gwangjin–gu, Seoul, South Korea

[2] Advanced Materials Program, Konkuk University, 120 Neungdong–ro, Gwangjin–gu, Seoul, South Korea

* Correspondence: mchoi@konkuk.ac.kr

Abstract

Copper is an indispensable trace element for maintaining metabolic homeostasis; however, the dysregulation and subsequent accumulation of Cu^{2+} are critically linked to neurodegenerative pathologies, including Alzheimer's disease in humans. Consequently, the development of robust analytical tools for Cu^{2+} monitoring is of paramount importance. Here, we report a 2,2′-dipicolylamine porphyrin (DPAP) based fluorescent sensor designed for the precision detection of metal cations. Photophysical investigations reveal that DPAP operates via a rapid turn-off fluorescence mechanism, achieving high-performance sensing in the parts-per-million range. Notably, the probe demonstrates exceptional sensitivity with a detection limit of 30.3 nM for Cu^{2+} and 34.8 nM for Ni^{2+}. Interference studies further confirm the superior selectivity of DPAP for Cu^{2+} over a broad spectrum of competing metal ions. These findings highlight DPAP as a simple, yet highly sensitive and selective probe for environmental monitoring and biomedical diagnostics involving copper ions.

Keywords: porphyrin sensor; fluorescence; 2,2′-dipicolylamine; metal cation; copper(II) ion

1. Introduction

Heavy and transition metals are significant environmental pollutants, yet they are essential for the vital functions of many organisms. However, by exposure to these metals both excess and deficiency can disrupt metabolic homeostasis or lead to environmental toxicity [1–4]. Due to their inherent toxicity, the precise detection and quantification of these metals are crucial. Fluorescence-based sensors have emerged as highly sensitive and efficient probes for this purpose; consequently, various chemosensors for metal cations have been developed [1,3,5–17]. Copper (Cu) is one of the most pervasive transition-metal contaminants. As a key micronutrient and the third most abundant transition metal in the human body [18], approximately 40 μg/L is required for normal metabolism [1,2,8]. Conversely, high concentrations of Cu can induce vomiting, nausea, diarrhea, hepatic or renal damage, and even fatality. Furthermore, Cu is suspected of causing liver damage in infants, and elevated Cu^{2+} levels are implicated in the pathogenesis of Alzheimer's disease [19]. Therefore, the quantification of trace Cu^{2+} ions is of paramount importance. Highly sensitive fluorescence-based methods have attracted significant attention for the detection of metal trace [9,18]. Various fluorophores, such as BODIPY [8,20], rhodamine [21,22], coumarin [23], benzimidazole [24–26], and naphthalimide [27,28], have been utilized. Among them, porphyrins having a π-conjugated macrocyclic ring and a planar conformation show intense visible light absorption and fluorescence emission. Porphyrins currently are widely applied in photodynamic therapy, organic solar cells, catalysis, and chemosensors [30–33].

 doi:10.20944/preprints202604.0723.v1

In this study, we report the synthesis of a novel fluorescence-based probe, 2,2′-dipicolylamine porphyrin (DPAP), designed for the detection of metal ions, particularly Cu^{2+}. This sensor features a porphyrin fluorophore substituted with 2,2′-dipicolylamine (DPA) at the meso position. In the DPAP system, the porphyrin acts as the signaling unit, while the DPA moiety serves as the metal-recognition unit. Notably, the high selectivity of DPA for Cu^{2+}, achieved through direct N–metal interactions, results in fluorescence quenching via intramolecular charge transfer (ICT) [5,29].

2. Results and Discussion

2.1. Synthesis and Characterization

To achieve high-performance fluorescence sensing, the fluorophores must have high quantum efficiency and photostability after metal binding. In addition, to overcome photon attenuation, fluorophores with long emission wavelengths, especially in the near-infrared (NIR) region, are preferred. Porphyrins have been used as fluorophores in fluorescence sensors for many metal ions. Crucially, porphyrin fluorophores have large Stokes shifts between the absorption (approximately 400 nm) and red/NIR emission [33–35]. Further, the DPA ligand forms stable complexes with many metal cations, resulting in high sensitivity [36]. In particular, we selected DPA because it can efficiently ligate metals in tridentate binding mode. Further, we assumed that, after coordination with a metal, the lone pair on nitrogen would not be available for conjugation, and fluorescence would be quenched. A previous study showed that DPA attached to a TPP moiety selectively reacted with Cd^{2+}; however, we expected a different result from the DPP-based DPAP sensor because it has a twisted structure, unlike that of TPP [12].

The synthesis of compounds **1–3** is shown in Scheme 1 and follows a literature method [30,31]. DPAP (**3**) was synthesized by Lindsey cross-coupling condensation, combining two aldehydes and DPM, followed by oxidation [37]. The synthesis of DPAP was confirmed by MALDI-TOF MS and ^{1}H-NMR spectroscopy (Figures S1 and S2).

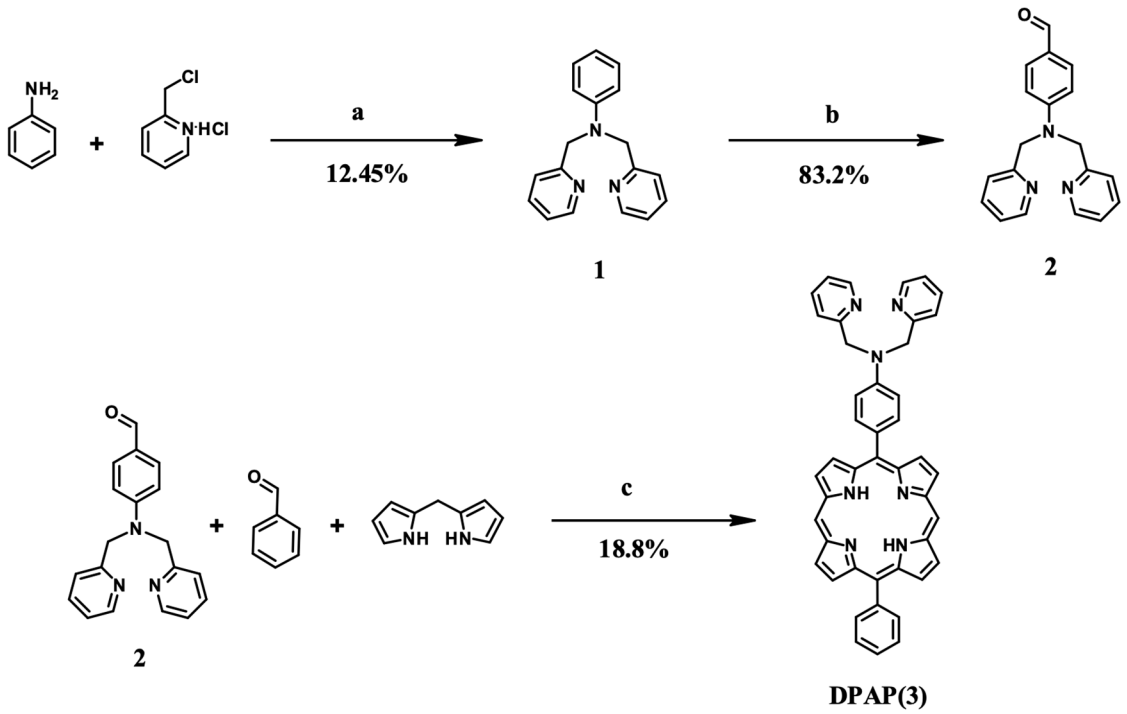

Scheme 1. Synthesis of DPAP (**3**). Reaction conditions: (a) Hexadecyltrimethylammonium chloride, water, 5 N NaOH/r.t, 24 h; (b) $POCl_3$, DMF/90 ℃, 2 h; (c) DCM, TFA/r.t, 6 h; chloranil/1 h; TEA/15 min.

 doi:10.20944/preprints202604.0723.v1

2.2. Optical Properties

A stock solution of DPAP was prepared in THF, and all photochemical experiments were carried out at a concentration of 1.5 × 10^{-5} M. Free DPAP produced a prominent absorption band peak maximum at 407 nm (Soret band), attributed to S_0–S_2 absorption, and four Q bands at 506, 546, 583, and 639 nm, attributed to S_0–S_1 electronic transitions. In addition, DPAP yielded fluorescence emissions at 647 and 706 nm when excited at 407 nm in THF [29,38]. Regarding the DPP reference, without DPA, DPP exhibited a Soret band at 405 nm and four Q bands at 501, 534, 576 m, and 633 nm. DPP showed fluorescence emissions at 635 and 700 nm when excited at 405 nm in THF solution.

At the same concentration in THF, the absorption spectra of DPP and DPAP differed (Figure 1(a)): the Soret band of DPAP was broadened, and the peak was red-shifted compared with those of DPP, possible because of the electron-donating ability of the DPA moiety toward the porphyrin ring.

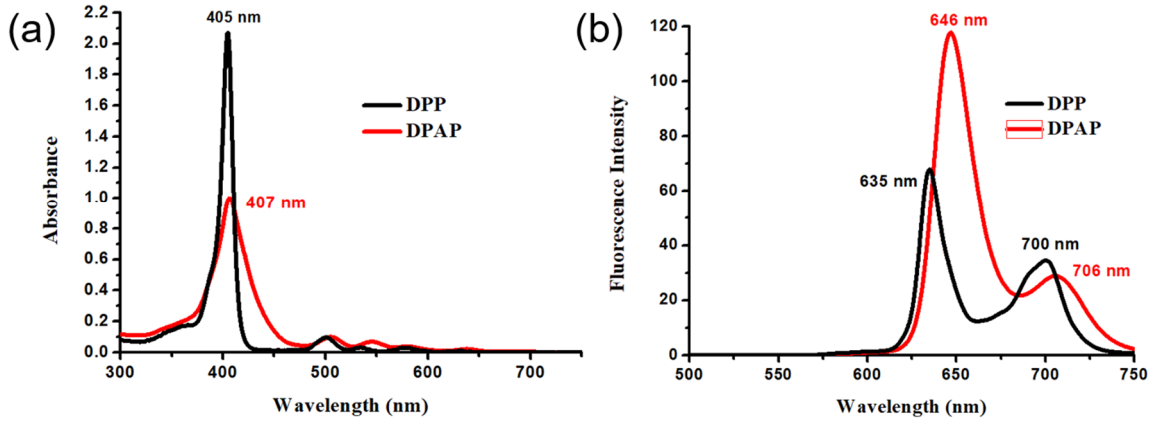

Figure 1. Absorption (a) and emission (b) (λ_{ex} = 407 nm) spectra of DPP and DPAP in THF (1.5 × 10^{-5} M).

2.3. Effect of Metal Ions on the Absorption and Emission of DPAP

To observe the photophysical response to various metal cations, the UV–vis and fluorescence spectra were measured in the presence of perchlorate salts of Na^+, Ag^+, Cu^{2+}, Ni^{2+}, Cr^{3+}, Pb^{2+}, Al^{3+}, Fe^{2+}, Cd^{2+}, and Zn^{2+}.

As shown in Figure 2(a), the Soret band is sharpened, and a hyperchromic shift occurs on metal-ion binding. The spectra for each ion are presented in order of peak intensity. The slight blue-shift suggests that M^{2+}/DPA coordination decreased the electron-donating ability of DPA, reducing the efficiency of ICT from the DPA subunits to the porphyrin fluorophore. In addition to this electron-withdrawing effect induced by the cations, M^{2+}/DPA coordination via the nitrogen might distort the porphyrin ring, decreasing the conjugation of the DPA moiety and fluorophore.

 doi:10.20944/preprints202604.0723.v1

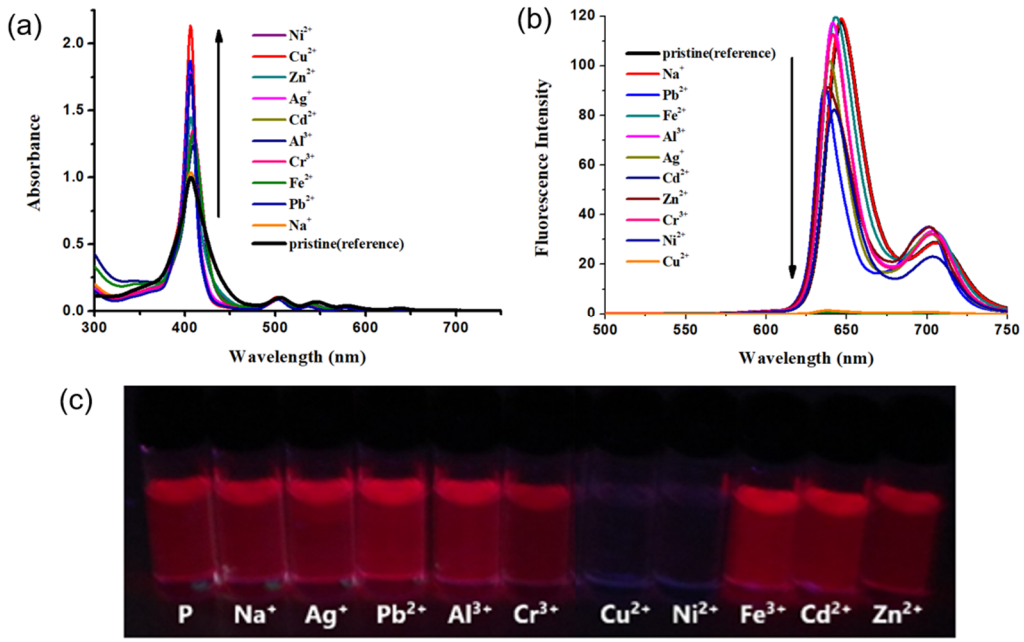

Figure 2. Absorption (a) and emission (b) spectra (λ_{ex} = 407 nm) and images (c) under UV light (λ_{em} = 365 nm) of DPAP (1.5×10^{-5} M) in the presence of various metal ions (1.5×10^{-4} M, 10 eq).

Next, the emission spectra of the sensors were measured at an excitation wavelength of 407 nm. Figure 2(b) shows that the fluorescence intensity is reduced by the coupling of the porphyrin sensor with various metals. The spectra for each ion are presented in order of peak intensity. The metal ions are chelated by the DPA functional group, and this depends on the size of the ion and its binding affinity.

In Figure 2(a), there remain four distinct Q bands, indicating that the metal ions do not bind to the porphyrin ring, and this is consistent with their high affinity for DPP. As shown in Figure S3, the UV–vis and fluorescence spectra of DPP showed no changes in the presence of metal cations, indicating that the DPA groups are the binding sites.

In the case of fluorescence, a slight metal-ion-dependent change was observed; however, a significant quenching was observed in the presence of Cu^{2+}, and Ni^{2+}. This is because the bite angle of DPAP is commensurate with the size of these metal ions. Figure 2(c) shows visible-light images of DPAP under UV light (λ_{em} = 365 nm), revealing considerable fluorescence quenching in the presence of Cu^{2+}, and Ni^{2+}. Therefore, we focused on the use of the DPAP-based sensor for Cu^{2+}, and Ni^{2+} detection.

The fluorescence quantum yields of DPAP after the addition of Cu^{2+}, and Ni^{2+} were calculated using the reference standard TPP (QY = 0.11). The quantum yield of DPAP before the addition of metal cations was 0.1018, and after the addition of Cu^{2+}, and Ni^{2+} the corresponding quantum yields of DPAP-Cu^{2+}, and DPAP-Ni^{2+} were 0.0016, and 0.0033 respectively. Further, the fluorescence quenching percentages of DPAP after the addition of Cu^{2+}, and Ni^{2+} were 99.1%, and 98.5% respectively. In terms of quenching and quantum yield changes, DPAP exhibited the highest reactivity towards Cu and Ni ions.

The titration of DPAP with increasing concentrations of Cu^{2+} led to a decrease in the emission intensity, as shown in Figure 3. No further changes were observed beyond the addition of 0.5 eq. The titration of DPAP with Ni^{2+} led to fluorescence quenching (Figure S4).

 doi:10.20944/preprints202604.0723.v1

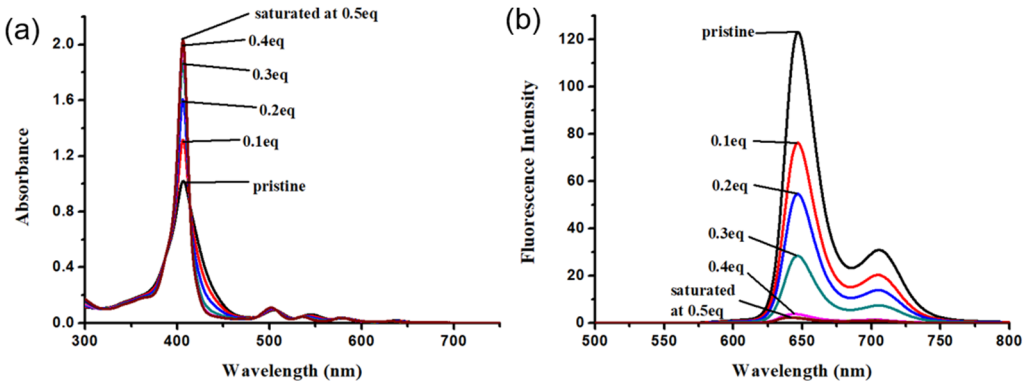

Figure 3. Absorption (a) and emission (b) (λ_{ex} = 407 nm) spectra of DPAP (1.5 × 10^{-5} M) with increase in Cu^{2+} concentration (1 eq = 1.5 × 10^{-5} M).

The LOD of DPAP for the two metal ions in THF was calculated from a linear fit of the maximum emission intensity at 647 nm and the quencher concentration (Figures S5–S6). The calculated LODs are 26.3, and 34.8 nM (≈ 2.0 ppb, R^2 = 0.98), respectively, for Cu^{2+}, and Ni^{2+} based on Eq. (1).

2.4. Binding Stoichiometry and Binding Affinity

To understand the binding behavior and determine the stoichiometry of the DPAP-Cu^{2+} complex, Job's plot analysis was carried out [6] (Figures S7–S8). The changes in the emission intensity ($I_0 - I$) at 647 nm versus the mole fraction of Cu^{2+} were measured while maintaining the concentrations of Cu^{2+} and DPAP at 1.5 × 10^{-5} M. The maximum change in emission intensity was observed at a molar fraction of approximately 0.5–0.6. In addition, in the case of Ni^{2+}, the results show that the DPA-based sensor for Ni^{2+} metal ion form 1:1 metal–ligand complexes.

As shown in Figures 4, and S9 near-linear Stern–Volmer plots were obtained at low quencher (metal ion) concentrations; these plots were used to investigate the "kinetics" of the quencher binding affinity. Linear fitting yielded a coefficient of determination (R^2) of > 0.99, and the obtained Stern–Volmer constants were 1.39 × 10^6, and 7.71 × 10^5 M^{-1}, respectively, for Cu^{2+}, and Ni^{2+} indicating an increase in binding affinity in that order.

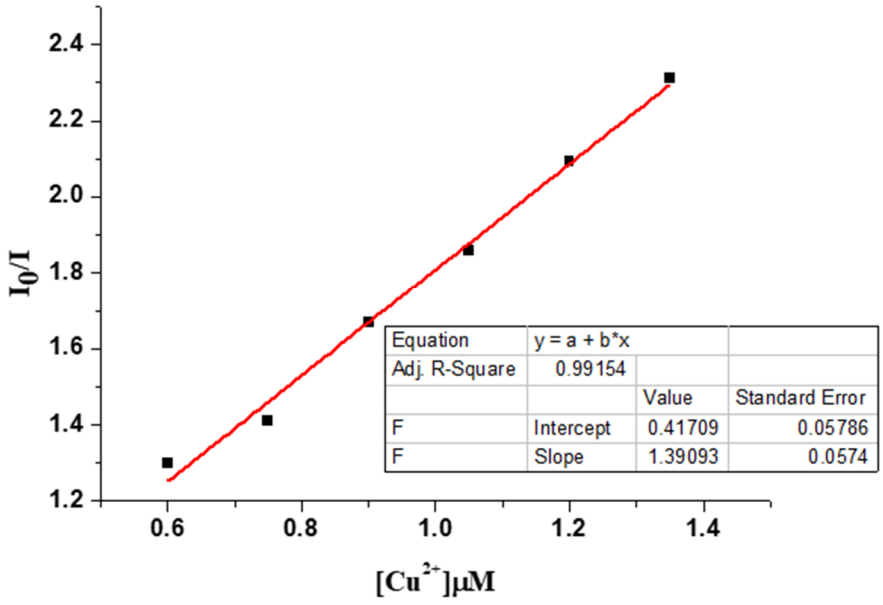

 doi:10.20944/preprints202604.0723.v1

Figure 4. Stern–Volmer plot of the quenching emission at 647 nm on the interaction of DPAP with Cu^{2+} (K_{sv} = 1.39 × 10^6 M^{-1}).

Next, interference (matrix) effects were investigated using metal cations proven to bind to the DPA moiety, such as Zn ions [12,13,39–46]. A comparative study was carried out by measuring at a low concentration (1 eq) mixture of Cu^{2+}, and Ni^{2+} and a high concentration (10 eq) of the interfering metal mixture. As shown in Figure 5, Cu^{2+} completely quenched the fluorescence, unlike the other metals, and no interference was observed. Although Ni^{2+} quenched the fluorescence, interference was observed in the presence of the metal mixture, and the fluorescence intensity increased again because of its low binding affinities. These results clearly demonstrate the high specificity of our sensor for Cu^{2+}, even in a complex matrix of metal ions.

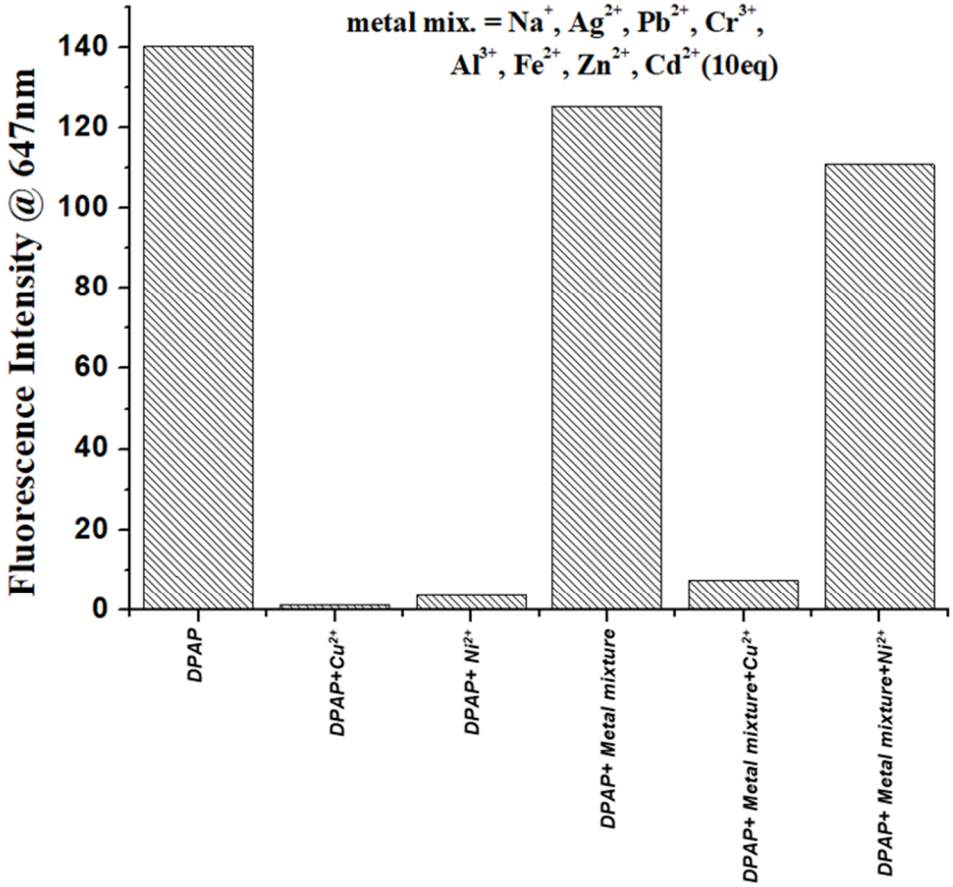

Figure 5. Fluorescence emission response of DPAP (1.5 × 10^{-5}M) in the presence of Cu^{2+}, and Ni^{2+} (1 eq) and interference effects in the presence of a metal mixture (10 eq).

To investigate the interference effect of each metal ions and metal ion mixtures on the detection ability of DPAP for Cu^{2+}, and Ni^{2+} the fluorescence response was measured in the presence of other metal ions (Figure 5 and Figures S10–S11). Exposure of DPAP to a mixed metal-ion solution containing Na^{+}, Ag^{2+}, Pb^{2+}, Cr^{3+}, Al^{3+}, Fe^{2+}, Zn^{2+}, and Cd^{2+} (10 equivalents each) does not significantly alter the fluorescence intensity, which remains comparable to that of the free DPAP. In contrast, addition of Cu^{2+} to the mixed-metal system, quenched the fluorescence of DPAP, highlighting the high selectivity of DPAP for Cu^{2+} even under competitive conditions. The addition of Ni^{2+} to the mixed-metal system results in partial quenching. In addition, DPAP has greater selectivity for Cu^{2+} than for Ni^{2+} ions as shown in Figures S10 and S11. Taken together these results highlight the Cu^{2+}selective fluorescence quenching exhibited by DPAP, underscoring its potential utility as a highly selective fluorescent probe for Cu^{2+} detection.

 doi:10.20944/preprints202604.0723.v1

Moreover, the optical response of DPAP to Cu^{2+} is fully reversible. In addition, when ethylenediaminetetraacetic acid (EDTA) was added to the complex solution, the fluorescence signal at 647 nm completely recovered (Figure 6) [14].

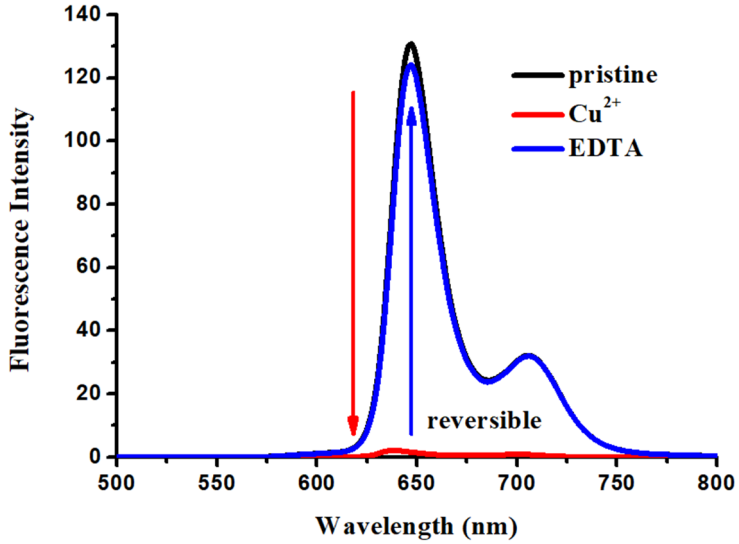

Figure 6. Emission spectra (λ_{ex} = 407 nm) of the DPAP-Cu^{2+} complex (1.5×10^{-5} M) in the presence of EDTA.

3. Experimental

3.1. Materials

All chemicals for synthesis were purchased from commercial suppliers and used as received. Aniline, phosphorus(V) oxychloride, and all metal salts were purchased from Sigma–Aldrich. Hexadecyltrimethylammonium chloride, benzaldehyde, dipyromethane (DPM), and chloranil were purchased from TCI. Picolyl chloride hydrochloride was purchased from Acros Organics. *N*,*N*′-Dimethylformamide (DMF) and dichloromethane (DCM) were purchased from Samchun Company. Trifluoroacetic acid (TFA) was purchased from Daejung Corporation. Triethylamine (TEA) was purchased from Duksan Corporation.

3.2. Measurements

^{1}H-NMR spectra were recorded at 600 MHz and are reported using the standard abbreviations: s: singlet, d: doublet, t: triplet, m: multiplet, and the coupling constants, *J*, are given in hertz. The chemical shifts are reported in parts-per-million (ppm), using tetramethylsilane (0 ppm) and $CDCl_3$ as standards. UV−vis absorption and fluorescence emission spectra were recorded using a Shimadzu UV-2450 spectrometer and Hitachi F-7000 fluorescence spectrophotometer, respectively. The slit size for excitation and emission was 5 mm. The emission spectra were measured with excitation at 407 nm. All spectra were recorded at room temperature (r.t.) in a quartz cuvette having a path length of 10 mm.

A stock solution of DPAP was prepared in tetrahydrofuran (THF) at a concentration of 1.5×10^{-5} M for excitation and emission measurements and stored in a cold, dark place before use. To test the sensing performance and interference effects, various metal-ion solutions (Na^+, Ag^+, Cu^{2+}, Ni^{2+}, Cr^{3+}, Pb^{2+}, Al^{3+}, Fe^{2+}, Cd^{2+} and Zn^{2+} as perchlorate salts) were prepared in water. Column chromatography was performed on Merck silica gel (230–400 mesh).

3.3. DPAP Synthesis

Compounds **1** and **2** were synthesized following literature procedures [30,31]. Compound **2** (DPA aldehyde) (0.519 g, 1.712 mmol), benzaldehyde (0.18 mg, 1.712 mmol), and DPM (0.5 g, 3.424

 doi:10.20944/preprints202604.0723.v1

mmol) were dissolved in dichloromethane (DCM; 600 mL), and the mixture was degassed for 10 min by sparging the solution with N_2. After the addition of TFA (0.234 g, 0.6 eq), the resulting solution was stirred at room temperature for 6 h in the dark. To this reaction mixture, chloranil (1.05 g, 4.28 mmol) was added, and the reaction mixture was stirred for another 1 h at r.t. After reaction completion, the mixture was neutralized with TEA (4 mL), filtered through a Büchner funnel filled with silica gel, and washed with chloroform, completing the work-up process. The crude compound **3** (i.e., DPAP) was purified by silica-gel column chromatography using chloroform (0.5% v/v methanol) as the eluent, yielding a magenta solid in 18.8% yield. ^{1}H-NMR (600 MHz, chloroform-*d*) δ = 10.281 (s, 2H, meso), 9.374 (d, 4H, J = 4.677 Hz, β), 9.179 (d, 2H, J = 4.402 Hz, β), 9.058 (d, 2H, J = 4.677 Hz, β), 8.7045 (d, 2H, J = 4.402 Hz, aromatic), 8.274–8.259 (m, 2H, aromatic), 8.083(d, 2H, J = 8.528 Hz, aromatic), 7.844–7.794 (m, 5H, aromatic), 7.5975 (d, 2H, J = 7.703Hz, aromatic), 7.297–7.285(m, 2H, aromatic), 7.161 (d, 2H, J = 8.528 Hz, aromatic), 5.126 (s, 4H, aliphatic), and -3.047 (s, 2H, NH).

Matrix-assisted laser desorption/ionization–time-of-flight mass spectrometry (MALDI-TOF-MS) measurements were conducted, and the weight of the target molecule (m/z) was calculated for $C_{44}H_{33}N_7$ $[M+H]^+$: 660.283; found: 660.471.

3.4. Limit of Detection

The limit of detection (LOD) was calculated using fluorescence titration with Eq. (1).

$$LOD = 3\sigma/k \quad (1)$$

Here, σ is the standard deviation of the emission intensity of DPAP, and k is the slope of the emission intensity plotted against the concentration. To determine the signal-to-noise ratio, the emission intensity of pristine DPAP without metal ions was measured four times, and the standard deviation of the blank measurements was determined to be 0.221736. Three independent duplicate measurements of the emission intensity were performed in the presence of Ni^{2+}, and Cu^{2+} and the average value of each intensity was plotted as a function of cation concentration to determine the slope.

3.5. Quantum Yield Measurements

The quantum yield was calculated using Eq. (2).

$$QY = \frac{I}{I_R} \times \frac{A_R}{A} \times \frac{\eta^2}{\eta_R^2} \times QY_R \quad (2)$$

Here, QY and QY_R are the quantum yields of the sample and reference, respectively, A and A_R are the absorbances of the sample and reference, respectively, and I and I_R are the areas of the emission peaks for the sample and reference, respectively. Tetraphenyl porphyrin (TPP), which has a quantum yield of 0.11, was used as a reference.

3.6. Binding Constants and Stoichiometry

The binding (K_{sv}) and quenching constants for the interaction of the metal cations with the probe were determined using Stern–Volmer plots, Eq. (3) (Keizer, 1983) [32].

$$\frac{I_0}{I} = 1 + K_{sv}[Q]_q \quad (3)$$

Here, I_0 is the initial emission intensity of DPAP before the addition of the quencher, I is the emission intensity at a given concentration of quencher Q ([Q]), and K_{sv} is the Stern–Volmer constant.

In addition, Job's plots were constructed to determine the stoichiometry of the complexation process between the metal ions and dye ligand [6,9,32]. In the plots, the x-axis represents the mole fraction, which is the ratio of the cation concentration to the total concentration of DPAP and cations. The total molar concentrations of the probe and metal ion were constant (1.5×10^{-5} M), and the difference in the emission intensity difference ($I_0 - I$) between DPAP and the DPAP–M^{2+} complex at 647 nm versus the mole fraction was measured.

 doi:10.20944/preprints202604.0723.v1

4. Conclusions

A novel fluorescence-based sensor, DPAP, was successfully synthesized by coupling a DPA metal-recognition moiety to a porphyrin fluorophore for the detection of transition metals, with a primary focus on Cu^{2+}. The sensor shows 'turn-off' fluorescence, where the addition of less than 1.0 molar equivalent amount of Cu^{2+} ions was sufficient to induce complete fluorescence quenching. The sensor achieved a limit of detection (LOD) of approximately 2.0 ppb for both Cu^{2+} and Ni^{2+}, demonstrating its potential for trace-level monitoring. Our results from quantum yield and Stern–Volmer analyses revealed the quenching efficiency of $Ni^{2+} < Cu^{2+}$, suggesting the high affinity of the DPAP probe for Cu^{2+} ions. Interestingly, DPAP exhibited selectivity for Cu^{2+} even in a mixture of metal ions. Altogether, our findings reveal that our porphyrin-based DPAP sensor is not only a robust tool for determining Cu^{2+} traces but is also a useful probe for detecting Cu^{2+} in complex aqueous environments.

Supplementary Materials: The following supporting information can be downloaded at the website of this paper posted on Preprints.org, Figure S1: MALDI-TOF MS of DPAP; Figure S2: ^{1}H-NMR spectrum of DPAP; Figure S3: Absorption and emission spectra of DPP in the presence of various metal ions; Figures S4: Absorption and emission spectra of DPAP titration in the presence of Ni^{2+} ion; Figures S5–S6: LODs of DPAP; Figures S7–S8: Job's plots of DPAP; Figures S9: Stern–Volmer plot of DPAP; Figures S10 and S11: Interference effects of different metal ions (10 eq).

Author Contributions: So-Hyun Shin: Methodology, Investigation and Synthesis. Jihyun Kim: Investigation and Synthesis. Hyungkyu Moon: Investigation and Synthesis. T. Sheshashena Reddy: Investigation, Characterization & Writing. Myung-Seok Choi: Conceptualization, Data curation, Funding acquisition, Resources, Project administration, Writing, Review, & Editing.

Funding: This work was supported by the Technology Innovation Program [No. 20026593 & No.00418987] funded by the Ministry of Trade, Industry & Energy (MOTIE, Korea). This paper was supported by Konkuk University Researcher Fund in 2024.

Institutional Review Board Statement: Not applicable.

Informed Consent Statement: Not applicable.

Data Availability Statement: All data and material described in this work are available in this article or in the Supplementary Materials.

Conflicts of Interest: The authors declare no conflicts of interest.

References

1. Sie, Y.W., Li, C.L., Wan, C.F., Yan, H., Wu, A.T., A novel fluorescence sensor for dual sensing of Hg^{2+} and Cu^{2+} ions, *J. Photochem. Photobiol. A Chem.* **353** (2018) 19–25.
2. Nekouei, F., Nekouei, S., Determination of copper, nickel and cobalt in water and food samples by FAAS after separation and preconcentration using multiwalled carbon nanotubes modified by methyl-(2-pyridyl) ketone oxime, *J. Anal. Chem.* **8** (2014) 138–145.
3. Neupane, L.N., Oh, E.T., Park, H.J., Lee, K.H., Selective and sensitive detection of heavy metal ions in 100% aqueous solution and cells with a fluorescence chemosensor based on peptide using aggregation-induced emission, *Anal. Chem.* **88** (2016) 3333–3340.
4. Momidi, B.K., Tekuri, V., Trivedi, D.R., Multi-signaling thiocarbohydrazide-based colorimetric sensors for selective recognition of heavy metal ions in aqueous medium, *Spectrochim. Acta A* **180** (2017) 175–182.
5. Zhou, X., et al., A highly selective fluorescent sensor for distinguishing cadmium from zinc ions based on a quinoline platform, *Inorg. Chem.* **51** (2012) 9226–9231.
6. Zhang, X., Wang, R., Fan, C., Liu, G., Pu, S., A highly selective fluorescent sensor for Cd^{2+} based on a diarylethene with a 1,8-naphthyridine unit, *Dyes Pigments* **139** (2017) 208–217.

 doi:10.20944/preprints202604.0723.v1

7. Cheng, T., et al., Red-emission fluorescent probe sensing cadmium and pyrophosphate selectively in aqueous solution, *Org. Lett.* **13** (2011) 3656–3659.
8. Baslak, C., Kursunlu, A.N., A naked-eye fluorescent sensor for copper(II) ions based on a naphthalene-conjugated BODIPY dye, *Photochem. Photobiol. Sci.* **17** (2018) 1091–1097.
9. Chae, J.B., et al., Highly sensitive dansyl-based chemosensor for detection of Cu^{2+} in aqueous solution and zebrafish, *ACS Omega* **4** (2019) 12537–12543.
10. Tian, Z., Cui, S., Pu, S., A highly selective fluorescent sensor for dual detection of Zn^{2+} and F^- based on a diarylethene, *Tetrahedron Lett.* **57** (2016) 2703–2707.
11. Chen, X., et al., Aggregation-induced emission enhancement-based ratiometric fluorescent sensor for detecting trace uranyl ion and application in living-cell imaging, *J. Lumin.* **186** (2017) 301–306.
12. Huang, W.B., et al., A porphyrin-based fluorescent probe for optical detection of toxic Cd^{2+} ion in aqueous solution and living cells, *Dyes Pigments* **143** (2017) 427–435.
13. Diana, R., et al., Data on a real-time tripodal colorimetric/fluorescence sensor for multiple target metal ions, *Data Brief* **19** (2018) 2119–2125.
14. Zhao, Q., et al., A highly selective on/off fluorescence sensor for cadmium(II), *Inorg. Chem.* **50** (2011) 10041–10046.
15. Surjeet, S., et al., 2-(2,2-Bis-benzylamino-1-cyano-vinyl)-benzonitrile: A Selective Turn-off Fluorescent Cu2+ Sensor, Chemistry Select 1 (2016) 2576–2580.
16. Li, Z.X., et al., Fluoranthene-based pyridine as a fluorescent chemosensor for Fe^{3+}, *Inorg. Chem. Commun.* **14** (2011) 1656–1658.
17. Han, A., Liu, X., Prestwich, G.D., Zang, L., Fluorescent sensor for Hg^{2+} detection in aqueous solution, *Sens. Actuators B* **198** (2014) 274–277.
18. Narayanaswamy, N., Govindaraju, T., Aldazine-based colorimetric sensors for Cu^{2+} and Fe^{3+}, *Sens. Actuators B* **161** (2012) 304–310.
19. Bagheri, S., Squitti, R., Haertlé, T., Siotto, M., Saboury, A.A., Role of copper in the onset of Alzheimer's disease compared to other metals, *Front. Aging Neurosci.* **9** (2018) 1–15.
20. He, X., et al., A BODIPY-based colorimetric and fluorometric dual-mode chemosensor for Hg^{2+} and Cu^{2+}, *Sens. Actuators B* **192** (2014) 29–35.
21. Kang, H., Fan, C., Xu, H., Liu, G., Pu, S., A highly selective fluorescence switch for Cu^{2+} and Fe^{3+} based on a diarylethene with a triazole-linked rhodamine 6G unit, *Tetrahedron* **74** (2018) 4390–4399.
22. Jin, X., et al., Dual-functional probe based on rhodamine for sequential Cu^{2+} and ATP detection in vivo, *Spectrochim. Acta A* **204** (2018) 657–664.
23. Shinde, R.G., et al., Fluorescence off–on signalling of esculetin in the presence of copper and thiol: implications in cellular thiol sensing, *Photochem. Photobiol. Sci.* **17** (2018) 1197–1205.
24. Tang, L., et al., Rapid and highly selective relay recognition of Cu(II) and sulfide ions by a benzimidazole-based fluorescent sensor in water, *Sens. Actuators B* **185** (2013) 188–194.
25. Hu, S., Zhang, S., Hu, Y., Tao, Q., Wu, A., A selective pyrazoline-based fluorescent chemosensor for Cu^{2+} in aqueous solution, *Dyes Pigments* **96** (2013) 509–515.
26. Tang, L., et al., Relay recognition of Cu^{2+} and S^{2-} in water by a benzimidazole-derived fluorescent sensor via ESIPT modulation, *Spectrochim. Acta A* **122** (2014) 656–660.
27. Fan, J., et al., A fluorescent ratiometric chemodosimeter for Cu^{2+} based on TBET and its application in living cells, *Org. Lett.* **15** (2013) 492–495.
28. Fu, Y., Fan, C., Liu, G., Pu, S., A colorimetric and fluorescent sensor for Cu^{2+} and F^- based on a diarylethene with a naphthalimide Schiff-base unit, *Sens. Actuators B* **239** (2017) 295–303.
29. Frangioni, J.V., In vivo near-infrared fluorescence imaging, *Curr. Opin. Chem. Biol.* **7** (2003) 626–634.
30. Sujatha, V., et al., Use of tetra-ammonium tetrakis(4-sulphonatophenyl) porphyrin for *Pseudomonas* and *Bacillus* cell imaging, *Int. J. Anal. Chem.* **2010** (2010) 697528.
31. Guo, B., et al., Decoration of porphyrin with tetraphenylethene: converting aggregation-caused quenching to aggregation-induced emission enhancement, *J. Mater. Chem. B* **4** (2016) 4690–4698.
32. Shiraishi, Y., Matsunaga, Y., Hirai, T., Selective colorimetric sensing of Co(II) in aqueous media using a spiropyran-amide-dipicolylamine linkage, *Chem. Commun.* **48** (2012) 5485–5487.

 doi:10.20944/preprints202604.0723.v1

33. Ahn, S.H., et al., Novel cobalt(II) complexes containing N,N-di(2-picolyl)amine-based ligands: synthesis, characterization and application in methyl methacrylate polymerisation, *J. Mol. Struct.* **1113** (2016) 24–31.
34. Song, Y., et al., Cadmium(II) complexes containing N′-substituted N,N-di(2-picolyl)amine ligands, *J. Organomet. Chem.* **783** (2015) 55–63.
35. Jeong, K., et al., Diisopropyl fluorophosphate degradation activity using transition-metal dipicolylamine complexes, *Appl. Organomet. Chem.* **32** (2018) e4041.
36. Bussey, K.A., et al., Synthesis, X-ray crystallography and catalytic activity of bis(2-pyridylmethyl)amine copper complexes in ATRA reactions, *Polyhedron* **114** (2016) 256–267.
37. Götzke, L., et al., Nickel(II) and zinc(II) complexes of N-substituted di(2-picolyl)amine derivatives, *Polyhedron* **30** (2011) 708–714.
38. Milaeva, E.R., et al., Redox-active metal complexes with dipicolylamine-ferrocenyl ligands, *J. Organomet. Chem.* **839** (2017) 60–70.
39. Azuma, Y., et al., Dipicolylamine as a structural switching element for helical peptides, *Org. Biomol. Chem.* **10** (2012) 6062–6068.
40. Praktikum, P., Quenching, F., Fluorescence quenching studies, *Phys. Prakt.* **1** (2016) 1–14.
41. Kumari, N., et al., Selective ppb-level detection of Cu^{2+} and Hg^{2+} using a micellar medium and application in cell imaging, *ChemPlusChem* **79** (2014) 1643–1652.
42. Zhang, L., et al., Fluorescent binary ensemble based on pyrene derivative and SDS assemblies for discriminating metal ions, *ACS Sens.* **2** (2017) 1821–1830.
43. Ncube, P., et al., Fluorescent sensing and determination of mercury(II) ions in water, *Water SA* **40** (2014) 175–182.
44. Milaeva, E.R., et al., Metal complexes with functionalised dipicolylamine ligands containing antioxidant moieties, *Dalton Trans.* **42** (2013) 6817–6828.
45. Lindsey, J.S., et al., Rothemund and Adler–Longo reactions revisited: synthesis of tetraphenylporphyrins under equilibrium conditions, *J. Org. Chem.* **52** (1987) 827–836.
46. Quantum Bioapplications, *An introduction to fluorescence spectroscopy*, Chem 312, (2007).